Chemical Engineering Journal 158 (2010) 89–99

Contents lists available at ScienceDirect

Chemical Engineering Journal

journal homepage: www.elsevier.com/locate/cej

Ethylene removal using biotrickling filters: part II. Parameter estimation and mathematical simulation

Sang-hun Lee*, Albert. J. Heber

Department of Agricultural and Biological Engineering, Purdue University, 225 South St., West Lafayette 47907-2093, IN, USA

ARTICLE INFO

Article history:
Received 3 January 2009
Received in revised form
15 November 2009
Accepted 21 December 2009

Keywords:
Biofiltration
Biotrickling filter
Ethylene (C_2H_4)
Genetic algorithm
Parameter estimation

ABSTRACT

Mathematical models of biofiltration often encounter uncertain parameters characterizing mass transfer, microbial degradation, biofilm growth, and biofilm detachment. The genetic algorithm, which is one of the most reliable methods for optimization although it has rarely been addressed in biofiltration models up to now, was utilized to estimate the unknown parameters using given experimental data. This study combined genetic algorithm and biofiltration equations to obtain simulated ethylene (C_2H_4) removal efficiencies with estimated parameters. Sensitivity analysis of each parameter was assessed to observe the significance of each parameter.

As a result, the simulation well characterized C_2H_4 removal efficiencies for most of the reactors. The large difference in removal efficiencies among reactors could be mostly explained using the mass transfer parameters. Perlite biotrickling filters with low continuous liquid flow tended to increase C_2H_4 removal efficiencies, due to a large active surface area of biofilm facilitating C_2H_4 transfer from the gas to the biofilm phase. Conversely, most of the other reactors underwent relatively low C_2H_4 removal because of high liquid flow that generated a severe mass transfer limitation. The low C_2H_4 removal in the biofilters with discontinuous liquid recirculation flow, in spite of the lowest liquid flow rate was, probably caused by a low active microbial growth condition.

1. Introduction

Mathematical models have been developed and utilized to investigate the mechanisms and discriminate significant design and operation parameters on biofiltration. Diks and Ottengraf developed a biofiltration model for other pollutants to simulate the reaction in fixed film bioscrubbers based on the assumption of zero-order growth in microbial degradation [1,2]. Some previous studies focused on simulation and parameter estimation of biofiltration of alkane compounds which are insoluble in water. These also used a model to predict biofilter performance under a steady state condition [3–5]. Deshusses et al. studied dynamic simulation to predict short-term biofiltration performance with regard to the interaction between contaminants [6,7]. Alonso et al. utilized a dynamic mathematical model to predict the biodegradation of toluene with biotrickling filtration [8,9]. The model for toluene removal can incorporate the effects of free water flow and biomass accumulation on filter media. The concept of pseudo steady state can facilitate the simulation of contaminant removal according to microbial growth.

In spite of efforts to develop simulations for better understanding of biofiltration mechanisms, there are several challenges to implementing the current models. The first challenge is how to predict the distribution of biofilm mass, which is an important parameter that influences substrate biodegradation in biofilters. Unfortunately, there are no known methods for accurately determining the parameter. The assessment of biofilm mass distribution is complicated by several factors such as non-uniformity of biofilm coverage over media and the presence of inactive biofilm in contaminant transfer and degradation [10].

Another challenge is to specify the kinetics of biodegradation. The estimation of kinetic parameters for the biological reactions taking place in the biofilter is not straightforward. Experimental data from batch reactors was used to easily obtain microbial kinetic information in biofiltration [9]. However, as Spigno and de Faveri reported [11], the biofilm formation of continuous reactions is often different from that of batch reaction.

While mathematical models of biofilters are complicated due to the high uncertainty of the parameters as stated above, inverse modeling offers a way to estimate them. If a proper set of experimental data is provided, estimation of the unknown parameters with a high degree of certainty can be identified using the inverse modeling approach. One of the most common methods for optimization is utilizing the derivative function for gradient search such as Newton, Levenberg-Marquardt, and Conjugate gradient methods

* Corresponding author. Tel.: +1 765 490 4242; fax: +1 765 496 1115.
E-mail address: lee323@purdue.edu (S.-h. Lee).

1385-8947/$ – see front matter © 2009 Elsevier B.V. All rights reserved.
doi:10.1016/j.cej.2009.12.034

Nomenclature

C_{Ai}	concentration of i substrate in the gas phase ($mg\,m^{-3}$)
C_{in}	inlet ethylene level entering the upper part of the media in a reactor ($mg\,m^{-3}$)
C_{Li}	concentration of i substrate in the gas phase ($mg\,m^{-3}$)
C_t^{exp}	experimentally measured ethylene concentration at time t ($mg\,m^{-3}$)
$C_{z,t}$	ethylene concentrations at depth z and time t ($mg\,m^{-3}$)
$C^B_{z,x,t}$	ethylene concentration in the biofilm phase at media depth z, biofilm depth x, and time t ($mg\,m^{-3}$)
D	diffusion constant of ethylene in the liquid or the biofilm phase ($m^2\,s^{-1}$)
df_n	degree of freedom for daily ethylene removal efficiency during the normal loading
df_{tran}	degree of freedom for ethylene removal efficiency during the transient loading
df_{pr}	degree of freedom for ethylene removal efficiency during the profile study
H	total media depth of the reactor (=50 cm) (m)
K_{AO}	ethylene partition coefficient between air and octanol phases
k_a	lumped mass transfer parameter of ethylene ($m^2\,m^{-3}$)
k_d	biofilm detachement/deactivation rate (h^{-1})
K_h	half saturation coefficient of the ethylene in the biofilm phase ($mg\,m^{-3}$)
k_L	$=X/Y$ ($mg\,m^{-3}$)
L	biofilm depth (or thickness) (m)
L_0	biofilm depth (or thickness) on day 92 (m)
Maxno	maximum of generation number
MSE	mean square error to be minimized by the genetic algorithms
Re	ethylene removal efficiency
S_i	concentration of i substrate in the biofilm phase ($mg\,m^{-3}$)
t	reaction time (s, h, or day)
V	the lumped ethylene biodegradation parameter ($mg\,m^{-3}\,h^{-1}$)
V'	$=V/K_h$ (h^{-1})
w_n	weight constant for normal loading
w_{tr}	weight constant for transient loading
w_{pr}	weight constant for the profile study
X	density of microbial cells of ethylene degradation ($mg\,m^{-3}$)
x	spatial variable for biofilm depth (or thickness) (m)
Y	yield coefficient
z	spatial variable on media depth (m)

Greek symbols

μ_{max}	specific microbial degradation rate (h^{-1})
ξ	an arbitrary random value ranging from zero to unity

Genetic symbols

$P(1,J,k)$	k_a(BHF-L) ($m^2\,m^{-3}$)
$P(2,J,k)$	k_a(BHF-M) ($m^2\,m^{-3}$)
$P(3,J,k)$	k_a(BHF-H) ($m^2\,m^{-3}$)
$P(4,J,k)$	k_a(BF) ($m^2\,m^{-3}$)
$P(5,J,k)$	k_a(BHF-GB) ($m^2\,m^{-3}$)
$P(6,J,k)$	k_d(BHF-L) (h^{-1})
$P(7,J,k)$	k_d(BHF-M) (h^{-1})
$P(8,J,k)$	k_d(BHF-H) (h^{-1})
$P(9,J,k)$	k_d(BF) (h^{-1})
$P(10,J,k)$	k_d(BHF-GB) (h^{-1})
$P(11,J,k)$	k_L ($mg\,m^{-3}$)
$P(12,J,k)$	V' (h^{-1})
$P(13,J,k)$	L_0 (m)

[12,13]. All these methods should use either analytical expressions or numerical approximations of the derivatives to find the optimal solution [12,13]. Unfortunately, those often fail to find the global optimized solution from non-linear equations with numerical iteration.

On the other hand, non-gradient-based optimization methods not requiring derivatives rely on finding optimal solutions only by memorizing previous estimates of parameters [13,14]. The genetic algorithm is one of the most popular methods in non-gradient-based optimization [14–16]. Unfortunately, there is no method that can definitely obtain a globally optimized solution for a non-linear function. However, many problems on global optimization have been successfully solved by the use of the genetic algorithm.

Some previous applications of the inverse model approach using the genetic algorithm concentrated on the characterization of conventional bioprocesses such as fermentation [17–19], and several studies were for biofiltration [10]. Bhat et al.'s evolutionary algorithm was applied to biofiltration modeling for analyzing the phenol degradation parameters and simulated removal [10]. Rene et al.'s studies utilized the neural network model to construct an empirical correlation to machine learning. This model predicts biofiltration performance directly from the biofilter design input values such as inlet contaminant concentrations and gas flow velocity [20,21].

The primary objective of the present study is to develop an efficient genetic algorithm for estimating unknown parameters that control C_2H_4 biodegradation. To achieve this goal, the genetic algorithm should be combined with the biofiltration model. The experimental data in the study of Lee and Lee et al. [22,23] were provided as input data for the parameter estimation procedure. The mathematical equations that simulate the biofiltration processes, including mass transfer, biodegradation, and biofilm growth, were modified from those of Alonso et al. [8,9], which is one of the most applicable models to the long-term unsteady state condition of biotrickling filtration used in this present study. The resulting algorithm is implemented as a computer program and applied to simulate C_2H_4 removal over time.

2. Mathematical model

2.1. Mass transfer of C_2H_4 through active surface

It is assumed that gas and liquid in the reactor are moved via convection transport along the vertical direction of a reactor in the co-current flow condition. The chemical i in the gas phase (C_{Ai}) is transferred into liquid phase (C_{Li}) and diffused into biofilm phase (S_i). The biodegradable contaminants in the biofilm phase are eliminated by microbial degradation.

Fig. 1a–c illustrates the concentration gradients of contaminants in the two or three phases of a biotrickling filter. In Fig. 1a, hydrophilic contaminants can easily be transferred through the liquid phase. The gradient of the concentrations of hydrophilic contaminants in the biofilm phase depends on mass transfer, diffusion, and microbial uptake.

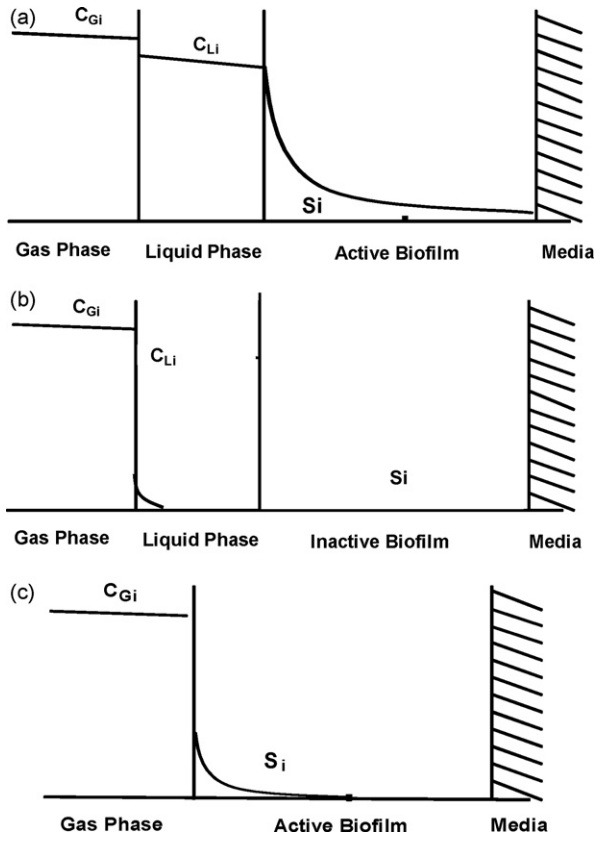

Fig. 1. Concentration gradients in two or three phases for hydrophilic contaminants through liquid flow (a), hydrophobic contaminants with liquid flow as barrier (b), and hydrophilic/hydrophobic contaminants without liquid barrier (c).

Fig. 1b shows that a hydrophobic compound cannot be transferred to the biofilm phase, because of mass transfer resistance under the presence of thick liquid films (e.g. when trickle liquid recirculation flow rates are excessive). Fig. 1c demonstrates the mass transfer of hydrophobic gaseous contaminants on biofilm-covered media surfaces in the absence of the thick liquid film. The surface is referred to as active surfaces in this study. If the contaminant is insoluble in water but easily absorbed to the biofilm, there are possible ways for removal of the contaminants by direct contact of the gaseous contaminant to the active biofilm surface, which is achieved by optimizing the trickle liquid flow rate to minimize liquid film thickness [23,24].

2.2. Assumptions

The following simplifying assumptions were made for the simulation:

(1) There is no chemical reaction between compounds of contaminants except interactions by microbial reaction.
(2) Temperature and viscosity of gas (air) and liquid (water) are constant.
(3) There are no nutrient or oxygen limitations to microbial growth.
(4) There is no effect of pH on C_2H_4 removal.
(5) The mass transfer between gas/liquid interfaces is always in equilibrium.
(6) The active surface area of a reactor is invariant throughout the entire operation.
(7) There is no multi-dimensional change in biofilm formation such as spreading.

2.3. C_2H_4 biofiltration equations

The dynamic mass transfer of C_2H_4 through a unit surface of media can be described as follows:

$$\frac{\partial C_{z,t}}{\partial t} = -v\frac{\partial C_{z,t}}{\partial z} - k_a D \frac{\partial C^B_{z,x,t}}{\partial x}|_{y=L_{z,t}} \quad (1)$$

BC 1: At $z = 0$, $C_{0,t} = C_{in}$

BC 2: $C_{H,t} = C_t^{\exp}$

BC 3: $\frac{C_{z,t}}{K_{AO}} = C^B_{z,L,t}$

BC 4: $\frac{\partial C_{z,x,t}}{\partial x}|_{x=0} = 0$

The variable $C_{z,t}$ represents the concentrations of C_2H_4 at depth z and time t. The variable $C^B{}_{z,x,t}$ means the C_2H_4 concentration in the biofilm phase. Since C_2H_4 is sparingly soluble to water, no C_2H_4 molecule in the liquid phase was assumed. The unknown parameter k_a ($m^2\ m^{-3}$) is a characteristic parameter related to C_2H_4 mass transfer through the active surface area of the biofilm-covered media and should be estimated using the experimental data. The coefficient D is the diffusivity of C_2H_4 in the liquid or the biofilm phase. The C_2H_4 diffusivity in the water (or biofilm) phase could be estimated as 1.71×10^{-5} cm^2/s using the Wilke-Chang method [25].

As for the boundary conditions, the value C_{in} means the inlet C_2H_4 level entering the upper part of the media in a reactor. The outlet C_2H_4 concentrations should be estimated to be equal to the measured level as much as possible. $C_t{}^{exp}$ is experimentally measured data. H is the total media depth of the reactor (50 cm). The third boundary condition described is the phase transfer between the gas and the biofilm phases. For this, the coefficient K_{AO} (Air–octanol partition), which is the C_2H_4 partition between air and octanol, can be used [26,27]. The last equation (BC4) shows the insulation boundary condition of ethylene diffusion on a solid media surfaces.

Both the diffusion and the microbial degradation of the C_2H_4 in the biofilm phase can be presented as follows:

$$\frac{\partial C^B_{z,x,t}}{\partial t} = D\frac{\partial^2 C^B_{z,x,t}}{\partial x^2} - V\frac{C^B_{z,x,t}}{K_h + C^B_{z,x,t}} \quad (2)$$

where K_h is the half saturation coefficient of the C_2H_4 in the biofilm phase. One can find that $C^B{}_{z,x,t}$ is also a function of x, the depth of the biofilm. The parameter V contains the specific microbial degradation rate (μ_{max}), the microbial cell density (X), and the yield coefficient (Y). The C_2H_4 degradation was assumed to follow first order kinetics using the parameter V' instead of the Monod-type equation, due to a high mass transfer limitation from gas to liquid (or biofilm) phases. Therefore, the second term of the right-hand side of Eq. (2) can be simplified as follows:

$$V\frac{C^B_{z,x,t}}{K_h + C^B_{z,x,t}} \approx V' \cdot C^B_{z,x,t} \quad (3)$$

$$V' = \frac{V}{K_h}$$

The dynamic change of the biofilm thickness at the media depth z in a reactor can be described as follows:

$$\frac{\partial L_{z,t}}{\partial t} = \frac{D}{k_L}\frac{\partial C^B_{z,x,t}}{\partial x}|_{x=L(z,t)} - k_d L_{z,t} \quad (4)$$

2.4. Genetic algorithm

The genetic algorithm is an optimal method for simulating the principles of genetics and evolution on natural selection. Along the genetic evolution, each chromosome (parameter set) consists of

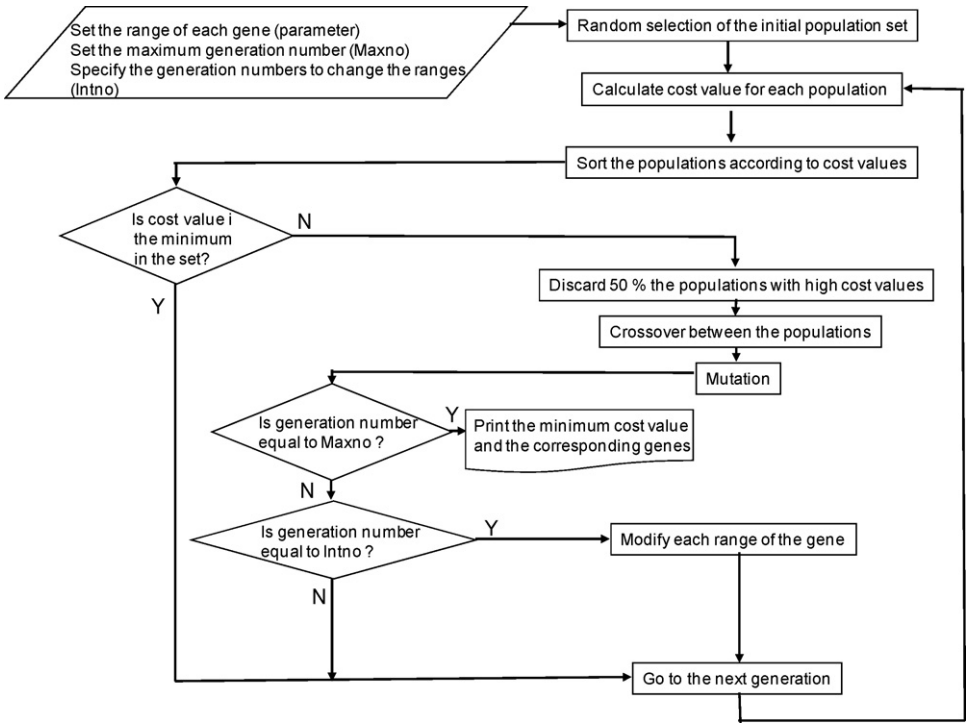

Fig. 2. Flowchart of the genetic algorithm for this study.

genes (parameters), and the chromosome is included in a population (a group of parameter sets) that exists in a generation (an iteration stage). Each parameter set undergoes evolution processes such as survival, extinction, mutation, or mating with other parameter sets throughout generations (stages). Based on certain criteria, some parameter sets with higher fitness for a given requirement are selected to survive in the generation but others become extinct, by the process of natural selection [14].

In an optimization approach to maximize fitness, a cost value, representing the fitness of each parameter set, is assessed. If the fitness is high (or the cost is low), the parameter set has an advantage in selection for mating and survival. Fig. 2 demonstrates the flow chart of the genetic algorithm designed for the parameter estimation for this study.

The first step was to generate a random initial population. One population consisted of 400 parameter sets. The initial values for the parameters were randomly specified.

$$P(i,j,0) = PL(i,j) + (PH(i,j) - PL(i,j)) \times \xi \quad (5)$$

where ξ is a random value ranging from zero to unity. Table 1 shows the list of parameters ($P(i,j,k)$), and their ranges ($PH(i,j)$ and $PL(i,j)$) which stand for the maximal and the minimal values of an estimated parameter.

Table 1
Unknown parameters and variables to be estimated using genetic algorithm.

Genes	Parameters	Low limit (PL)	High limit (PH)
$P(1,J,k)$	k_a(BHF-L)	10	1.00E+05
$P(2,J,k)$	k_a(BHF-M)	10	1.00E+05
$P(3,J,k)$	k_a(BHF-H)	10	1.00E+05
$P(4,J,k)$	k_a(BF)	10	1.00E+05
$P(5,J,k)$	k_a(BHF-GB)	10	1.00E+03
$P(6,J,k)$	k_d(BHF-L)	1	1.00E−03
$P(7,J,k)$	k_d(BHF-M)	1	1.00E−03
$P(8,J,k)$	k_d(BHF-H)	1	1.00E−03
$P(9,J,k)$	k_d(BF)	1	1.00E−03
$P(10,J,k)$	k_d(BHF-GB)	1	1.00E−03
$P(11,J,k)$	k_L	1	1.00E+10
$P(12,J,k)$	V'	1	1.00E+10
$P(13,J,k)$	L_0	1.00E−07	1.00E−04

The ranges were given prior to genetic algorithm modeling, and any estimated parameters during the modeling could not deviate out of the ranges. The specification of the ranges was helpful to avoid the estimations of parameters that were mathematically correct but physically unreasonable. Other constraints were that two duplicated reactors in each treatment set should have identical values for the parameters k_a and k_d and all reactors should have the same values for k_L, V', and initial biofilm thickness (L_0). Since the parameter k_a is closely related to the media specific surface area, the possible maximum value was equal to the total specific surface area of perlite ($10^5\ m^2\ m^{-3}$) or that of glass beads ($10^3\ m^2\ m^{-3}$). Perlite specific surface area from the literature is $3.5\ m^2\ g^{-1}$ [28]. This is much higher than the specific surface area of a glass bead ($\ll 0.001\ m^2\ g^{-1}$). However, perlite surface contains many micropores and mesopores as well as macro-pores [29]. The micro- and mesopores are usually unavailable for biofilm attachment and growth. Therefore, this study assumed only parts of the perlite surface can includes active biofilm.

The next step was to calculate the cost of each parameter set in the population. The mean square error (MSE) was used as the cost value that can be assessed as follows:

$$MSE = \frac{w_n \sum_{i=1}^{i=5} \sum_{t} (Re(i,t)^2_{n,\exp} - Re(i,t)^2_{n,\sim})}{df_n} + \frac{w_{tr} \sum_{itr=1}^{itr=3} \sum_{in=1}^{3} \sum_{t} (Re(itr,in,t)^2_{tr,\exp} - Re(itr,in,t)^2_{tr,\sim})}{df_{tran}} + \frac{w_{pr} \sum_{ipr=1}^{ipr=3} \sum_{id=1}^{3} \sum_{t} (Re(ipr,id,t)^2_{pr,\exp} - Re(ipr,id,t)^2_{pr,\sim})}{df_{pr}}. \quad (6)$$

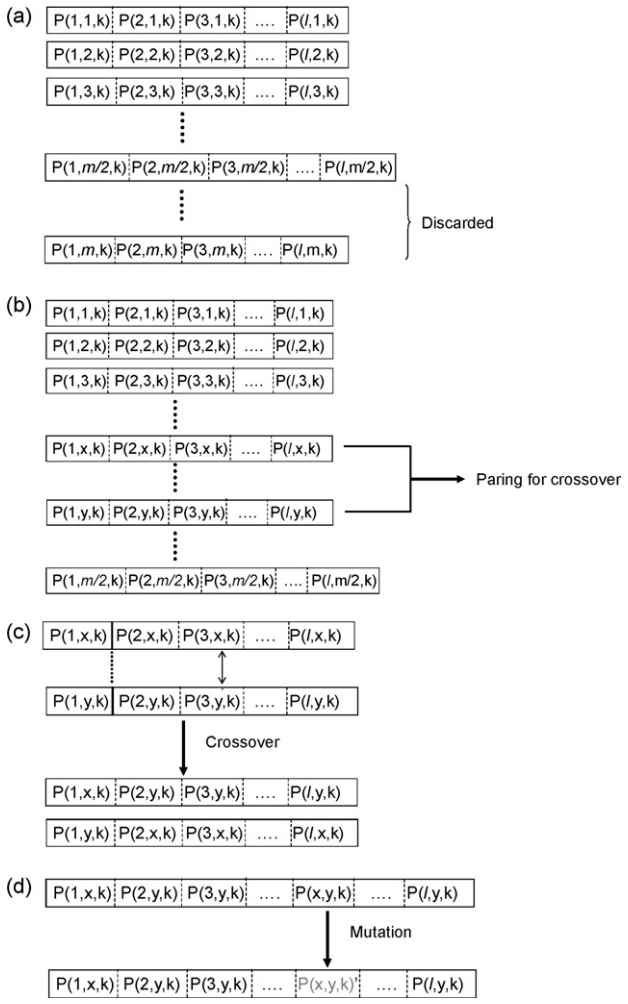

Fig. 3. The sub-processes of the genetic algorithm as gene extinction (a), pairing for crossover (b), crossover (c), and mutation (d).

The weight constant for normal loading w_n is unity, and those for the transient loading (w_{tr}) and the profile study (w_{pr}) are five, in order to reflect the high significance of the data on transient loading and the profile studies. The variable $Re(x,t)$ means C_2H_4 removal efficiency at arbitrary dataset x on day t. Each of the degree of freedom for the data of the normal operation, the transient loading, and the profile study are denoted as df_n, df_{tran}, or df_{pr}, respectively. A low resultant *MSE* means a high fitness. The weighting factor of a unity was given to calculate *MSE* for the C_2H_4 removal efficiencies under normal loading.

Next, some individual parameter sets from the current population were selected to generate an offspring (n individuals) by copying its own parameters. In this study, 50% of parameter sets, those with low fitness in a generation, were discarded and not considered for mating in the next generation (Fig. 3a). The pairing was made by random selection of any two parameter sets (Fig. 3b). The crossover points were randomly chosen for the mating of a pair of parameter sets (Fig. 3c). The mutation was given by selecting one gene and changing the value to a different one within the range specified in Table 1 (Fig. 3d). The probability of the selection for the mutation was 0.1.

The maximum generation number (*Maxno*) was set as 500 in this study, which was decided empirically. At generation numbers 200 and 400, the minimum value of each parameter was limited to 0.9% to 0.95% of the optimal parameter values, respectively. The maximum value was 1.1 and 1.05 times the optimal parameter values, respectively. This was helpful to reduce the computation time for the global optimization in the parameter estimation.

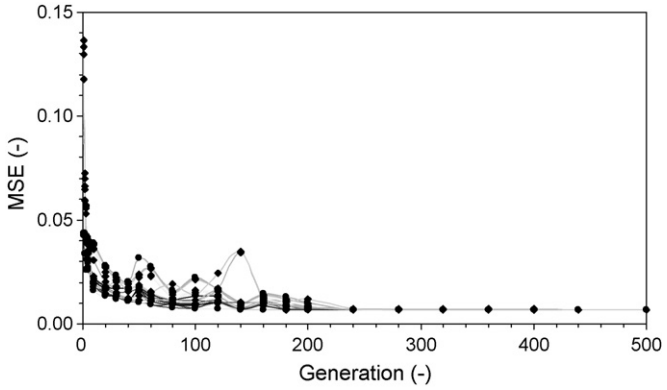

Fig. 4. Variation of mean squared errors between measured and simulated ethylene removal for each population as influenced by generation.

After the major parameter estimation task stated above, the genetic algorithm was implemented for each single reactor, and consequentially, each parameter was estimated for only a single set. The objective of the work was to check the validity of the assumption that the respective parameters V', k_L, and the variable L_0 are identical over all reactors, if a minimized *MSE* is obtained via convergence resulting from the iteration, the corresponding parameters are optimally estimated. All of the computations including the genetic algorithm and the biofiltration model were programmed using C language in Microsoft Visual Studio software.

3. Results and discussion

3.1. Minimization of MSE

The parameter estimation using the genetic algorithm was conducted with a total 821 data sets, each set produced C_2H_4 removal efficiencies for all reactors. Some of the resultant *MSE* according to the generation elapsed are presented in Fig. 4. The computation time for the genetic algorithm was about 23–28 s per generation. Since the genetic algorithm is inherently stochastic, the global optimization was not guaranteed with a single implementation. Hence, as shown in Fig. 4, the best 20 chromosomes with low costs were selected based on results from 10 independent implementations of the genetic algorithm. Each implementation was completely independent of the others. Table 2 exhibits the variation of *MSE* of the 20 parameter sets, with low *MSEs* for each generation stage, and Table 3 shows the value of each parameter in the set with the lowest *MSE* for each generation.

The costs decreased greatly during early generation. The costs of the first generation were 0.042–0.14 but those decreased to 0.016–0.020 by the 10th generation. At the 200th generation, all chromosomes converged around 0.007. Optimization of the minimal cost was confirmed by the gradient-based optimization previously used [8,9]. The average costs from the first to the 199th generation were 0.06–0.10, which varied only slightly with each elapsed generation. However, after the 200th and the 400th generation, the average costs decreased to approximately 0.02 and 0.01, respectively. Such phenomena imply that the average costs were highly affected by the parameter ranges specified prior to the model implementation.

3.2. Simulated C_2H_4 removal

The results of the process model are shown in Fig. 5a–e with five treatment sets. The standard deviations of the model data

Table 2
MSE variation of the best 20 parameter sets as generation elapsed.

	0	1	2	3	4	5	10	20	30	40	50	60	80
1	4.25E−02	4.25E−02	3.36E−02	2.59E−02	2.59E−02	2.59E−02	1.59E−02	1.38E−02	1.18E−02	1.11E−02	1.02E−02	9.38E−03	7.76E−03
2	4.28E−02	4.25E−02	4.25E−02	3.36E−02	3.36E−02	2.66E−02	1.59E−02	1.38E−02	1.21E−02	1.13E−02	1.04E−02	9.38E−03	9.13E−03
3	4.35E−02	4.25E−02	4.27E−02	3.89E−02	3.36E−02	2.73E−02	1.77E−02	1.41E−02	1.29E−02	1.13E−02	1.04E−02	9.38E−03	9.13E−03
4	4.36E−02	4.27E−02	4.27E−02	4.10E−02	4.09E−02	2.96E−02	1.97E−02	1.41E−02	1.29E−02	1.14E−02	1.57E−02	9.38E−03	9.13E−03
5	4.37E−02	4.27E−02	4.27E−02	4.11E−02	4.11E−02	3.36E−02	2.06E−02	1.47E−02	1.35E−02	1.15E−02	1.60E−02	1.10E−02	9.30E−03
6	4.40E−02	4.28E−02	4.27E−02	4.12E−02	4.11E−02	3.36E−02	2.20E−02	1.74E−02	1.51E−02	1.15E−02	1.65E−02	1.27E−02	9.93E−03
7	4.42E−02	4.29E−02	4.28E−02	4.12E−02	4.12E−02	3.36E−02	2.30E−02	1.82E−02	1.51E−02	1.54E−02	1.67E−02	1.35E−02	1.06E−02
8	4.50E−02	4.33E−02	4.28E−02	4.13E−02	4.12E−02	3.36E−02	2.30E−02	1.82E−02	1.71E−02	1.74E−02	1.77E−02	1.38E−02	1.20E−02
9	4.52E−02	4.34E−02	4.30E−02	4.13E−02	4.12E−02	3.49E−02	3.05E−02	2.01E−02	1.77E−02	1.77E−02	1.77E−02	1.50E−02	1.20E−02
10	4.54E−02	4.37E−02	4.31E−02	4.16E−02	4.13E−02	3.52E−02	3.61E−02	2.29E−02	1.82E−02	1.78E−02	1.90E−02	1.54E−02	1.20E−02
11	4.60E−02	4.37E−02	4.32E−02	4.17E−02	4.17E−02	3.81E−02	3.63E−02	2.48E−02	2.04E−02	1.78E−02	2.23E−02	2.27E−02	1.26E−02
12	4.63E−02	4.38E−02	4.33E−02	4.20E−02	4.18E−02	4.06E−02	3.81E−02	2.69E−02	2.07E−02	1.79E−02	2.24E−02	2.32E−02	1.43E−02
13	4.68E−02	4.39E−02	4.33E−02	4.25E−02	4.18E−02	4.07E−02	3.87E−02	2.78E−02	2.15E−02	1.95E−02	2.35E−02	2.66E−02	1.50E−02
14	4.73E−02	4.39E−02	4.34E−02	4.25E−02	4.20E−02	4.09E−02	3.91E−02	2.83E−02	2.25E−02	2.02E−02	2.41E−02	2.73E−02	1.55E−02
15	4.74E−02	4.40E−02	4.35E−02	4.27E−02	4.20E−02	4.09E−02	3.92E−02	2.83E−02	2.36E−02	2.02E−02	3.19E−02	2.75E−02	1.59E−02
16	1.33E−01	1.18E−01	5.92E−02	3.14E−02	3.05E−02	3.05E−02	1.95E−02	1.66E−02	1.35E−02	1.15E−02	1.15E−02	1.13E−02	1.13E−02
17	1.36E−01	1.30E−01	6.46E−02	5.31E−02	3.11E−02	3.11E−02	1.95E−02	1.69E−02	1.46E−02	1.15E−02	1.15E−02	1.14E−02	1.13E−02
18	1.38E−01	1.33E−01	6.62E−02	5.56E−02	3.14E−02	3.44E−02	1.95E−02	1.70E−02	1.47E−02	1.18E−02	1.15E−02	1.15E−02	1.13E−02
19	1.40E−01	1.33E−01	6.98E−02	5.68E−02	3.88E−02	3.84E−02	1.95E−02	1.73E−02	1.47E−02	1.23E−02	1.36E−02	1.15E−02	1.13E−02
20	1.40E−01	1.36E−01	7.27E−02	5.75E−02	4.06E−02	3.97E−02	1.95E−02	1.75E−02	2.01E−02	1.67E−02	1.85E−02	1.55E−02	1.92E−02
	100	120	140	160	180	200	240	280	320	360	400	440	500
1	7.46E−03	7.41E−03	6.98E−03	6.87E−03	6.87E−03	6.86E−03	6.67E−03	6.61E−03	6.59E−03	6.59E−03	6.58E−03	6.58E−03	6.58E−03
2	7.46E−03	7.43E−03	7.03E−03	6.87E−03	6.87E−03	6.86E−03	6.68E−03	6.62E−03	6.59E−03	6.59E−03	6.58E−03	6.58E−03	6.58E−03
3	7.79E−03	9.83E−03	7.03E−03	6.87E−03	6.87E−03	6.86E−03	6.68E−03	6.62E−03	6.59E−03	6.59E−03	6.58E−03	6.58E−03	6.58E−03
4	7.80E−03	1.06E−02	7.11E−03	8.84E−03	6.87E−03	6.87E−03	6.68E−03	6.63E−03	6.59E−03	6.59E−03	6.58E−03	6.58E−03	6.58E−03
5	9.04E−03	1.06E−02	7.15E−03	8.94E−03	6.96E−03	6.88E−03	6.69E−03	6.64E−03	6.59E−03	6.60E−03	6.58E−03	6.58E−03	6.58E−03
6	9.45E−03	1.06E−02	7.42E−03	9.68E−03	7.17E−03	7.22E−03	6.71E−03	6.65E−03	6.59E−03	6.60E−03	6.58E−03	6.58E−03	6.58E−03
7	1.00E−02	1.14E−02	7.49E−03	9.80E−03	7.37E−03	7.45E−03	6.72E−03	6.65E−03	6.59E−03	6.63E−03	6.59E−03	6.58E−03	6.58E−03
8	1.34E−02	1.32E−02	7.99E−03	1.11E−02	8.57E−03	8.26E−03	6.72E−03	6.67E−03	6.60E−03	6.63E−03	6.59E−03	6.58E−03	6.59E−03
9	1.52E−02	1.33E−02	7.99E−03	1.15E−02	1.05E−02	8.54E−03	6.72E−03	6.67E−03	6.61E−03	6.63E−03	6.60E−03	6.58E−03	6.59E−03
10	1.53E−02	1.39E−02	8.73E−03	1.17E−02	1.06E−02	8.89E−03	6.73E−03	6.67E−03	6.62E−03	6.64E−03	6.60E−03	6.58E−03	6.59E−03
11	1.59E−02	1.43E−02	9.06E−03	1.24E−02	1.13E−02	8.96E−03	6.76E−03	6.69E−03	6.62E−03	6.64E−03	6.60E−03	6.58E−03	6.59E−03
12	1.63E−02	1.54E−02	9.25E−03	1.28E−02	1.14E−02	8.96E−03	6.76E−03	6.69E−03	6.62E−03	6.64E−03	6.61E−03	6.58E−03	6.59E−03
13	2.14E−02	1.67E−02	9.67E−03	1.37E−02	1.20E−02	9.92E−03	6.76E−03	6.69E−03	6.62E−03	6.66E−03	6.62E−03	6.58E−03	6.59E−03
14	2.20E−02	1.68E−02	9.78E−03	1.42E−02	1.22E−02	1.00E−02	6.76E−03	6.69E−03	6.64E−03	6.66E−03	6.62E−03	6.58E−03	6.60E−03
15	2.25E−02	1.69E−02	9.82E−03	1.48E−02	1.31E−02	1.07E−02	6.77E−03	6.71E−03	6.65E−03	6.68E−03	6.63E−03	6.58E−03	6.60E−03
16	1.13E−02	1.06E−02	1.06E−02	1.01E−02	8.49E−03	7.92E−03	7.50E−03	7.45E−03	7.29E−03	7.21E−03	7.18E−03	6.92E−03	6.84E−03
17	1.13E−02	1.06E−02	1.06E−02	1.06E−02	8.49E−03	7.92E−03	7.50E−03	7.46E−03	7.29E−03	7.21E−03	7.19E−03	6.92E−03	6.84E−03
18	1.13E−02	1.60E−02	1.06E−02	1.06E−02	8.69E−03	7.92E−03	7.50E−03	7.46E−03	7.30E−03	7.25E−03	7.19E−03	6.92E−03	6.84E−03
19	1.13E−02	1.70E−02	3.45E−02	1.18E−02	9.15E−03	8.59E−03	7.54E−03	7.50E−03	7.34E−03	7.25E−03	7.19E−03	6.92E−03	6.84E−03
20	1.42E−02	2.42E−02	3.48E−02	1.29E−02	1.07E−02	1.19E−02	7.54E−03	7.50E−03	7.38E−03	7.26E−03	7.25E−03	6.92E−03	6.84E−03

Table 3
Variation of the best parameter set with the lowest *MSE*, according to each generation.

	0	1	2	3	4	5	10	20	30	40	50	60	80
k_a(BHF-L)	1.25E+03	1.25E+03	1.76E+03	1.98E+03	1.98E+03	1.98E+03	1.98E+03	1.83E+03	1.83E+03	1.83E+03	2.07E+03	2.07E+03	3.41E+03
k_a(BHF-M)	7.02E+02	7.02E+02	6.99E+02	1.07E+03	1.07E+03	1.07E+03	1.07E+03	6.99E+02	6.99E+02	6.99E+02	1.14E+03	1.14E+03	1.14E+03
k_a(BHF-H)	9.50E+02	9.50E+02	9.32E+02	9.62E+02	9.62E+02	9.62E+02	9.34E+02	1.64E+03	1.64E+03	1.64E+03	1.64E+03	1.57E+03	1.38E+03
k_a(BF)	5.44E+02	5.44E+02	1.10E+03	8.57E+02	8.57E+02	8.57E+02	8.03E+02	1.10E+03	1.10E+03	1.10E+03	1.10E+03	1.10E+03	1.10E+03
k_a(BHF-GB)	1.17E+02	1.17E+02	8.07E+01	4.72E+01	4.72E+01	4.72E+01	1.68E+02	2.09E+02	7.10E+02	7.10E+02	7.10E+02	7.10E+02	7.10E+02
k_d(BHF-L)	5.66E−04	5.66E−04	1.29E−03	6.58E−04	6.58E−04	6.58E−04	1.40E−03	1.21E−03	1.21E−03	1.21E−03	1.21E−03	1.21E−03	1.21E−03
k_d(BHF-M)	7.10E−04	7.10E−04	1.10E−03	9.36E−04	9.36E−04	9.36E−04	9.97E−04	9.95E−04	9.95E−04	9.95E−04	1.02E−03	1.59E−03	1.59E−03
k_d(BHF-H)	1.24E−03	1.24E−03	1.82E−03	1.03E−03	1.03E−03	1.03E−03	1.80E−03	1.63E−03	1.63E−03	2.89E−03	1.40E−03	1.65E−03	1.65E−03
k_d(BF)	7.96E−04	7.96E−04	1.07E−03	8.08E−04	8.08E−04	8.08E−04	3.02E−03	3.37E−03	3.37E−03	4.44E−03	3.38E−03	3.38E−03	3.51E−03
k_d(BHF-GB)	8.43E−04	8.43E−04	8.94E−04	6.89E−02	6.89E−02	6.89E−02	1.12E−03	3.89E−03	3.89E−03	4.03E−03	3.95E−03	3.57E−03	3.76E−03
kL	1.25E+03	1.25E+03	7.95E+06	3.87E+06	3.87E+06	3.87E+06	5.79E+06	5.29E+06	5.29E+06	5.11E+06	5.47E+06	5.47E+06	5.38E+06
V'	1.11E+03	1.11E+03	1.26E+03	1.12E+03	1.12E+03	1.12E+03	1.21E+03	1.21E+03	1.21E+03	1.21E+03	1.21E+03	1.21E+03	1.21E+03
L_0	1.41E−06	1.41E−06	1.39E−06	1.00E−06	1.00E−06	1.00E−06	1.11E−06	9.64E−07	9.70E−07	9.98E−07	7.36E−07	7.40E−07	7.19E−07
MSE	4.25E−02	4.25E−02	3.36E−02	2.59E−02	2.59E−02	2.59E−02	1.59E−02	1.38E−02	1.18E−02	1.11E−02	1.02E−02	9.38E−03	7.76E−03
	100	120	140	160	180	200	240	280	320	360	400	440	500
k_a(BHF-L)	3.41E+03	3.41E+03	3.41E+03	3.41E+03	3.41E+03	3.41E+03	3.52E+03	4.57E+03	4.70E+03	4.70E+03	4.65E+03	4.65E+03	4.73E+03
k_a(BHF-M)	1.14E+03	1.14E+03	1.14E+03	1.14E+03	1.14E+03	1.14E+03	1.16E+03	1.16E+03	1.16E+03	1.16E+03	1.16E+03	1.16E+03	1.14E+03
k_a(BHF-H)	1.38E+03	1.38E+03	1.38E+03	1.38E+03	1.38E+03	1.38E+03	1.28E+03	1.25E+03	1.25E+03	1.25E+03	1.23E+03	1.24E+03	1.23E+03
k_a(BF)	1.10E+03	1.60E+03	1.53E+03	1.51E+03	1.51E+03	1.55E+03	1.78E+03	1.87E+03	1.95E+03	1.94E+03	1.92E+03	1.96E+03	2.03E+03
k_a(BHF-GB)	7.10E+02	6.22E+02	6.22E+02	5.87E+02	5.87E+02	5.87E+02	5.48E+02	5.15E+02	5.15E+02	5.15E+02	5.16E+02	5.11E+02	5.09E+02
k_d(BHF-L)	1.21E−03	1.21E−03	1.21E−03	1.25E−03	1.25E−03	1.25E−03	1.47E−03	1.91E−03	1.83E−03	1.82E−03	1.81E−03	1.83E−03	1.83E−03
k_d(BHF-M)	2.33E−03	2.22E−03	2.22E−03	2.41E−03	2.41E−03	2.41E−03	2.70E−03	2.59E−03	2.59E−03	2.59E−03	2.65E−03	2.66E−03	2.63E−03
k_d(BHF-H)	1.65E−03	1.71E−03	1.71E−03	1.80E−03	1.80E−03	1.80E−03	1.48E−03	1.19E−03	1.21E−03	1.22E−03	1.15E−03	1.15E−03	1.15E−03
k_d(BF)	3.51E−03	4.33E−03	4.40E−03	4.46E−03	4.46E−03	4.46E−03	4.74E−03	4.74E−03	4.77E−03	4.77E−03	4.80E−03	4.79E−03	4.85E−03
k_d(BHF-GB)	3.76E−03	3.90E−03	3.61E−03	3.87E−03	3.87E−03	3.87E−03	3.62E−03	3.38E−03	3.30E−03	3.31E−03	3.46E−03	3.27E−03	3.27E−03
k_L	5.38E+06	5.30E+06	4.66E+06	4.66E+06	4.66E+06	4.66E+06	4.48E+06	4.53E+06	4.54E+06	4.54E+06	4.54E+06	4.53E+06	4.52E+06
V'	1.21E+03	1.19E+03	1.19E+03	1.19E+03	1.19E+03	1.19E+03	1.19E+03	1.18E+03	1.19E+03	1.19E+03	1.19E+03	1.19E+03	1.19E+03
L_0	7.19E−07	8.76E−07	3.84E−07	3.98E−07	3.98E−07	3.98E−07	3.30E−07	3.51E−07	3.10E−07	3.07E−07	3.06E−07	3.07E−07	3.01E−07
MSE	7.46E−03	7.41E−03	6.98E−03	6.87E−03	6.87E−03	6.86E−03	6.67E−03	6.61E−03	6.59E−03	6.59E−03	6.58E−03	6.58E−03	6.58E−03

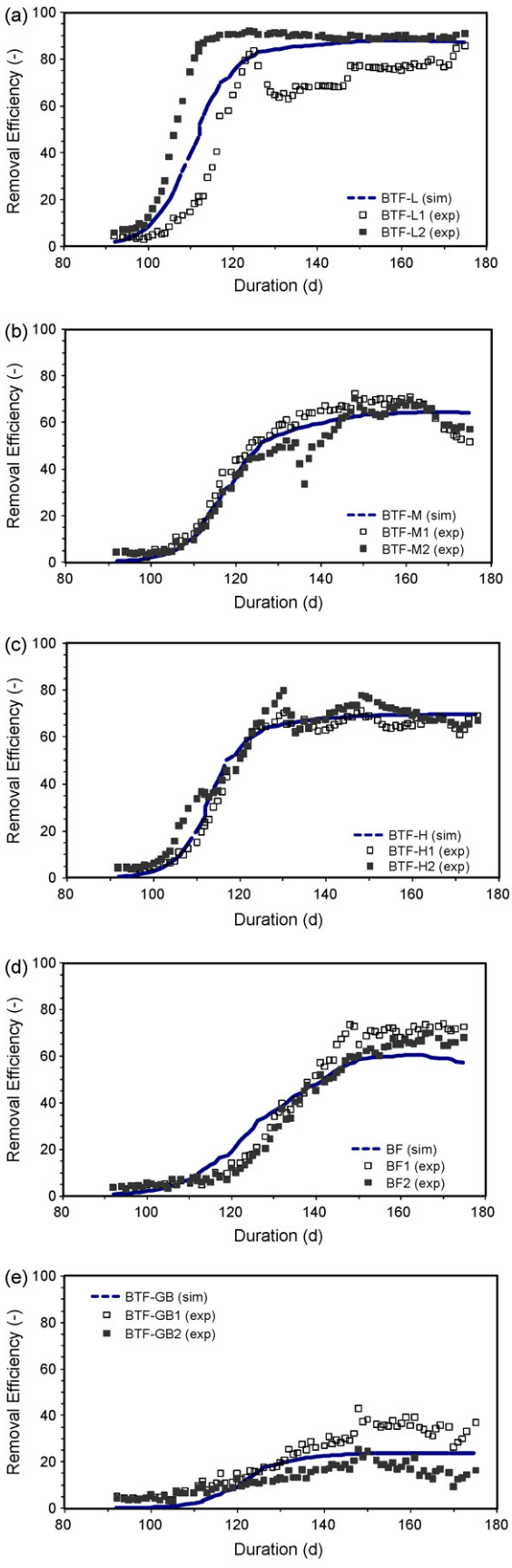

Fig. 5. Simulated (sim) and measured (exp) ethylene removal for BTF-L (a), BTF-M (b), BTF-H (c), BF (d), and BTF-GB (e) treatment sets.

from their corresponding measured data ranged from 4.0×10^{-3} to 1.6×10^{-2}. The small range of error implied that the numerical model generally provided a good fit of the experimental data. The simulated ethylene removal efficiencies during the initial period were lower than their corresponding experimental data. This is because the ethylene removal efficiencies were assumed to be zero on day 92, for the convenience in modeling.

The standard deviation for BTF-L was much larger than the others, because of a high difference of C_2H_4 removal between the two BTF-L reactors. The model seems to poorly simulate the ethylene removal of BF reactors, compared with other reactors. Unlike the perlite biotrickling filters, the ethylene removal efficiencies of the BF reactors were highly increased after day 110. It seems that BF reactors required longer adaptation periods than perlite BTF reactors.

The optimized estimation of each parameter was conducted together with the 95% of confidential intervals under the assumption that the error distribution around the estimated value of the parameter should follow the normal distribution with the mean as the estimated value.

This estimated parameter k_a (95% C.I.) was $6.22 \times 10^3 \pm 4.91 \times 10^3$, $1.51 \times 10^3 \pm 3.33 \times 10^2$, $1.62 \times 10^3 \pm 5.27 \times 10^2$, $2.67 \times 10^3 \pm 1.63 \times 10^3$, and $6.70 \times 10^2 \pm 2.03 \times 10^2$ $m^2\ m^{-3}$ for BTF-L, BTF-M, BTF-H, BF, and BTF-GB, respectively. The relatively high ranges of k_a for BTF-L reflect the large difference of C_2H_4 removal between BTF-L1 and BTF-L2. The physico-chemical meaning of the parameter k_a is specific media surface area that contains active biofilm exposed to ethylene gas. It is consequential that C_2H_4 removal can be expected to increase, as k_a increases. A high (or low) k_a can be obtained by a high (low) specific surface area of media, a high (low) biofilm-covered portion of the media surface area, and a low (or high) mass transfer limitation.

The major mass transfer limitation of ethylene in this study results from trickle liquid flow. However, the limitation effect is apparently not linearly correlated to the trickle liquid flow rates. For example, BTF-M and BTF-H have comparable k_a even though BTF-H reactors have much higher liquid recirculation rates. This is possibly related to liquid film thickness and wetted surface areas where liquid covered the surrounding biofilm. That is, although BTF-H had greater trickling liquid in the reactor, the BTF-M and BTF-H reactors may have had the similar limitation affect each other. The optimized values of the parameter k_d representing biofilm detachment and deactivation [9] were 1.83×10^{-3}, 1.26×10^{-3}, 1.15×10^{-3}, 4.85×10^{-3} and 3.47×10^{-3} h^{-1} for BTF-L, BTF-M, BTF-H, BF, and BTF-GB, respectively. The standard deviation for the k_d parameter could not be obtained for most of the reactor treatment sets, because the parameter sensitivity is relatively low (this will be discussed in the next section). As for other estimated parameters according to treatments, the lumped microbial degradation parameter V' was estimated as $1.19 \times 10^3 \pm 1.20 \times 10^2$ h^{-1}, k_L, which is the parameter denoting cell conversion and density, as $4.52 \times 10^6 \pm 5.41 \times 10^5$ $m^3\ mg^{-1}$, and initial biofilm thickness (L_0) as $3.01 \times 10^{-4} \pm 1.02 \times 10^{-4}$ mm.

Figs. 6a–e exhibit the results of the sensitivity study for parameters k_a, k_d, k_L, V', and L_0, as a result of estimations with five treatment sets. As shown in Fig. 6a, the BTF-L2 and BF reactors with low liquid recirculation rates had high k_a values. This implies that low liquid recirculation may provide a large biofilm surface exposed to the gas phase, which leads to high k_a. On the other hand, BTF-GB with the low biofilm exposed surface area had a low k_a. In this study, perlite is assumed to be 100 times higher in specific surface area active for biofilm attachment than glass beads, but k_a of BTF-L was just 10 times higher than that of BTF-GB. It probably because only large pores in perlite were available for the microbial habitat, even if small pores contribute to enlarging the media surface area [28,29]. The sensitivity for k_d shown in Fig. 6b was mostly low around the

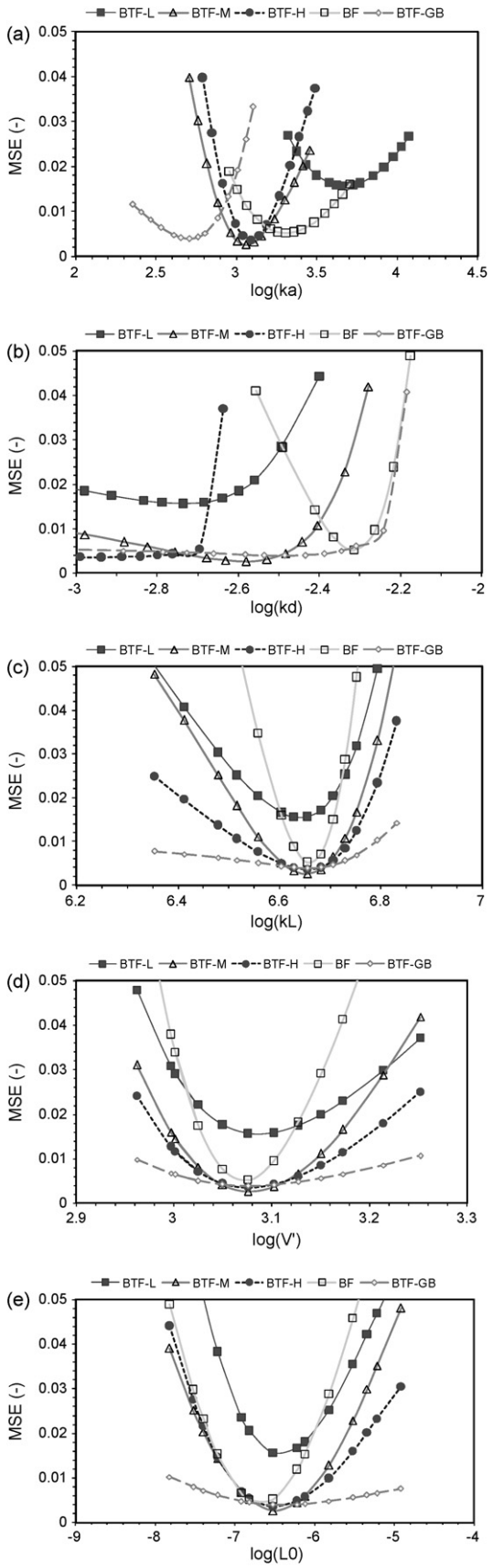

Fig. 6. The mean sum of errors between measured and simulated ethylene removal efficiencies as influenced by k_a (a), k_d (b), k_L (c), V' (d), and L_0 (e).

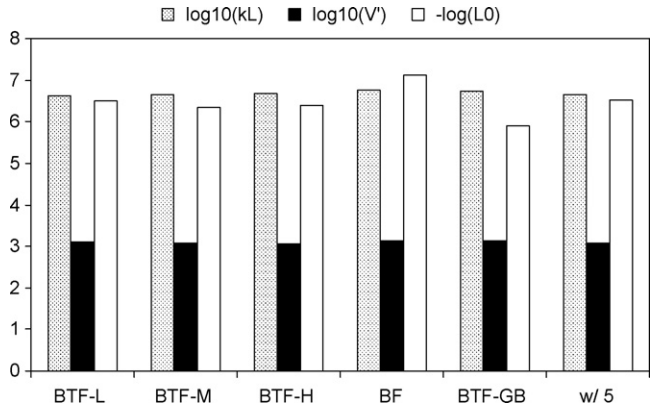

Fig. 7. Estimated parameters k_L and V', and the variables L_0 for each reactor (BTF-L to BTF-GB) and those for five treatment sets (w/5).

optimal values, although the sensitivity suddenly increased as k_d increased, which means biofilm detachment or deactivation [9] was severely affected by k_d only when its value is high. BF had a unique pattern in the sensitivity curve, with k_d because biofilm detachment significantly affecting the simulation prediction of C_2H_4 removal by BF. Actually, this parameter is a kind of nuisance parameter because the first term of the right-hand side of Eq. (4) is more decisive in biofilm thickness calculation on the left hand side of Eq. (4).

Fig. 6c–e presents the results of the parameter sensitivity for k_L, V', and L_0. The lumped microbial parameter V' was a highly sensitive parameter, which means the microbial degradation ability is one of the most influential factors in ethylene removal. The model by Deshusses et al. [6] also reported that when the effective coefficient is greater than 1.0 $m^2\ s^{-1}$, the elimination capacities (or removal efficiencies) of methyl ethyl ketone are highly affected by the increase of maximum degradation rates. The 10 times increase of maximum degradation rates leads to great increase of removal efficiencies from 10–15% to approximately 45%.

As stated earlier, the parameter estimations described above, was implemeted based on the assumption that the lumped microbial degradations and the microbial growth parameters were identical for all reactors, and checked by calculating all parameters based on entire five treatment sets. To check the reasonableness of the assumption, as presented in Fig. 7, this study newly estimated k_L, V', and initial biofilm thickness L_0 with each individual reactor treatment set. The vertical axis of the bar graph in Fig. 7 represents the values of $\log_{10}(k_L)$ for gray bars, $-\log_{10}(V')$ for black bars, and $-\log_{10}(L_0)$ for white bars.

Fig. 7 shows that k_L (4.14×10^6 to 5.60×10^6 mg m^{-1}) and V' (1.15×10^3 to 1.39×10^3 h^{-1}) exhibited little variation, but L_0 ranging from 7.78×10^{-5} to 1.27×10^{-4} mm showed a relatively large variation. In particular, as a result of the estimation with a single reactor set, BF reactors produced relatively different estimation results of k_L and L_0 (Figs. 5d and 6d versus Fig. 7). However, as for other the other sets, there was little difference between the five individual treatment sets.

This study provided information on the microbial degradability of C_2H_4. The parameter k_L means cell density divided by yield coefficient ($X{\cdot}Y^{-1}$), which is calculated as 4.4 g L^{-1} in this study. The lumped microbial degradation parameter divided by the parameter V'/k_L indicates the maximal specific microbial growth coefficient divided by the half saturation coefficient ($\mu_{max}\, K_h^{-1}$), corresponding to 6.2 $m^3\ d^{-1}\ g^{-1}$ and 5.65–7.26 $m^3\ d^{-1}\ g^{-1}$, based on estimation with five treatment sets and an individual treatment set, respectively.

Using toluene degradation in a biotrickling filter, Alonso et al. estimated 20 $m^3\ d^{-1}\ g^{-1}$ and 20 L g^{-1} for $V'{\cdot}k_L^{-1}$

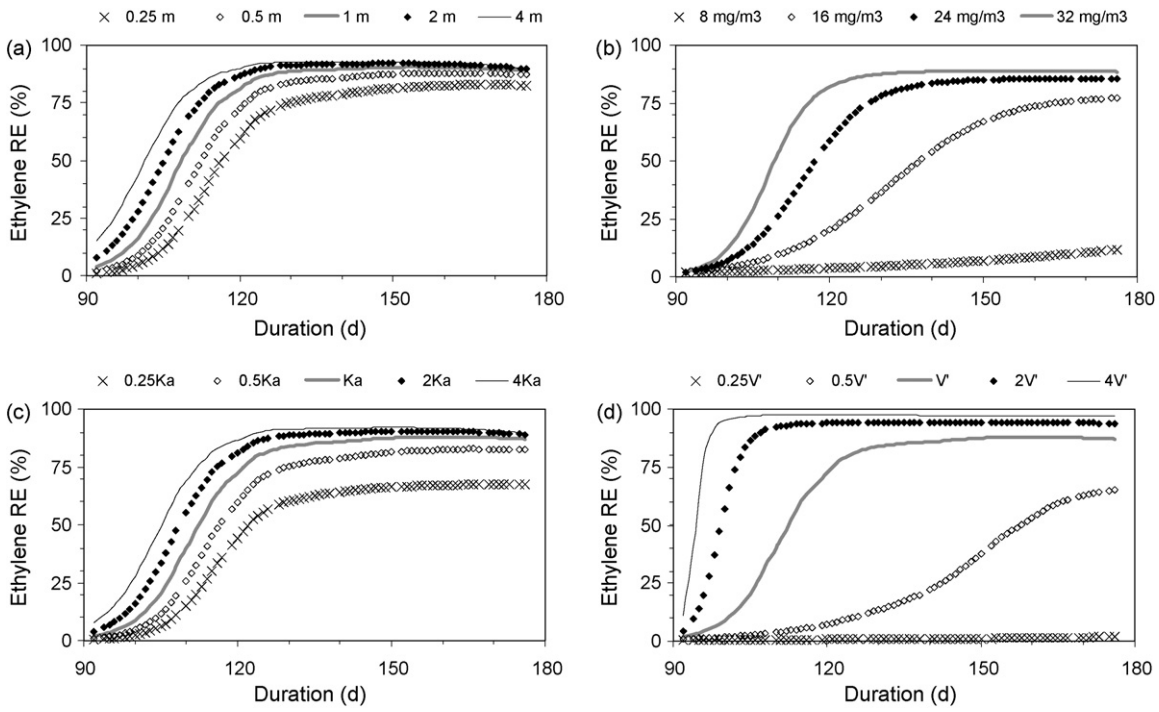

Fig. 8. Predictive ethylene removal efficiencies according to variation of media depth (a), inlet concentrations (b), the lumped mass transfer parameter (c), and the lumped microbial degradation parameter (d).

($=\mu_{max}/K_h^{-1}$) and k_L ($=X{\cdot}Y^{-1}$), respectively [8,9]. In Tabak et al.'s study on liquid phase bioremediation [30], M-xylene and benzene were estimated as 3.94 and 0.2 for V' k_L^{-1} ($=\mu_{max}{\cdot}K_h^{-1}$). This shows that the microbial degradability ($\mu_{max}{\cdot}K_h^{-1}$) of C_2H_4 is higher than M-xylene or benzene but lower than toluene. The parameter k_L ($X{\cdot}Y^{-1}$) of C_2H_4 is smaller than that of toluene, probably because of the low density of C_2H_4 degraders due to the co-existence of nitrifiers [31,32].

The carbon mass balance was simply established with outlet CO_2 concentrations and inlet C_2H_4 concentrations shown in the Lee's study [22], together with C_2H_4 removal efficiencies characterized in the present study. As a result, approximately 75% of carbon molecules in degraded C_2H_4 were converted to CO_2. Compared with other previous studies, almost complete conversion from C_2H_4 to CO_2 is usually expected, as in the studies of Elsgaard [33] and Kim [34], but the dynamic phase of C_2H_4 removal in this study may utilize a significant amount of C_2H_4 carbons for microbial cell construction. Also, it is possible that some of the 25% of C_2H_4 could be converted into incomplete oxidized compounds as ethanol or methyl-ketones other than CO_2 [35], or utilized for inactive microbial cell formation. The biofilm growth resulting from ammonia removal was not included in the simulation, because only little amounts of ammonia can be utilized for biofilm formation [22].

The predictive C_2H_4 removal efficiencies were influenced by variation of the media bed depth (Fig. 8a), inlet C_2H_4 concentrations (Fig. 8b), the lumped mass transfer parameter (k_a) (Fig. 8c), and the lumped microbial degradation parameter (V') (Fig. 8d). The predictive C_2H_4 removal and the parameter sets were obtained from the simulated data of BTF-L during days 152–176.

Fig. 8a shows that C_2H_4 removal increases as media bed depth increases (or EBRT increases). However, the improvement is small at a media depths greater than 1.5 m (or a gas flow rate less than 3.5 L min^{-1}), the improvement decreases. The C_2H_4 removal efficiencies measured at 0.25 m depth in the profile study were less than the corresponding predicted values shown in Fig. 8a [22]. The overestimation of the removal efficiencies in the simulation over the corresponding experimental data is probably due to the presence of activated nitrifiers at the upper part of the reactor, which led to possible inactivation of C_2H_4 degradation.

Fig. 8b exhibits the simulated C_2H_4 removal efficiencies according to C_2H_4 inlet concentrations. Such low inlet concentrations of 8 or 16 mg m^{-3} resulted in very low C_2H_4 removal efficiencies, due to low biofilm growth rates. The proposed simulation utilized first order kinetics to model C_2H_4 degradation and therefore could not be used with high inlet concentration ranges. Fig. 8c and d shows C_2H_4 removal efficiencies as influenced by k_a and V'. These graphs show that high k_a or V' is needed to increase C_2H_4 removal. Also, the effect of microbial degradation V' on C_2H_4 removal was greater than that of k_a. The parameter k_a can increase by using media with a highly specific surface area or optimized trickle liquid recirculation rates. The increase of the microbial parameter V' can be achieved by optimizing nutrients supply or applying microorganisms with a high C_2H_4 degradability [32,33].

As for the applicability of the genetic algorithm to biofiltration design and operation, it is useful for predicting reliable estimation values of the parameters in complicated theoretical equations. The accuracy of the prediction of biofiltration performance using the genetic algorithm is as high as that of the ANN model [20] by Rene et al. which utilized the artificial neural network algorithm. The ANN model, which enables a computer to recognize the input-output data pattern, can provide good prediction results within a short computation time but may give unrealistic solutions when the true output is not recognized on the basis of past input–output data pattern. The advantage of the modeling approach in this study over the ANN model is that inclusion of the theoretical equations for mass transfer and biodegradation enables wide ranges of scientific prediction. For example, an extrapolation to predict biofiltration is possible with only a small number of parameters. The disadvantage of the model in the proposed study is the high complexity in model construction and time-consuming in computation, because the genetic algorithm should deal with much more solution candidate than the ANN model.

4. Conclusions

A numerical model using a genetic algorithm was developed to estimate unknown parameters in C_2H_4 removal in biofiltration and related biofilm thickness changes. The model accounted for first order microbial degradation of C_2H_4 and an active media surface area resulting from the mass transfer limitation of gaseous C_2H_4 transfer. The experimental data predicted by the model consisted of C_2H_4 removal efficiencies with time of operation.

The parameters to be estimated were classified into two groups. The first is the group of parameters that have identical values over all reactors, including lumped parameters for microbial growth, C_2H_4 degradation, and initial biofilm thickness. The second group consisted of active specific surface area and a parameter for biofilm detachment, both of which were estimated differently according to five individual treatment sets.

The genetic algorithm was applied to find a global solution for optimal parameter estimation. The difference in C_2H_4 removal between reactors or modes was mostly explained by different values of k_a parameters. The high removal of C_2H_4 in the perlite biotrickling filters with a low liquid recirculation rate was caused by a large active surface area that facilitated C_2H_4 transfer from the gas to the biofilm phase. By contrast, other reactors suffered from low microbial activity or high mass transfer limitations.

Acknowledgement

Funding for this research was provided by Purdue-NSCORT (Advanced Life Support/NASA Specialized Center of Research and Training).

References

[1] R.M.M. Diks, S.P.P. Ottengraf, Verification studies of a simplified model for the removal of dichloromethane from waste gases using a biological trickling filter (Part II), Bioprocess Eng. 6 (3) (1991) 131–140.
[2] R.M.M. Diks, S.P.P. Ottengraf, Verification studies of a simplified model for the removal of dichloromethane from waste gases using a biological trickling filter (Part I), Bioprocess Eng. 6 (3) (1991) 93–99.
[3] J.W. Barton, B.H. Davison, K.T. Klasson, C.C. Gable III, Estimation of mass transfer and kinetics in operating trickle-bed bioreactors for removal of VOCs, Environ. Prog. 18 (2) (1999) 87–92.
[4] J.W. Barton, S.M. Hartz, K.T. Klasson, B.H. Davison, Microbial removal of alkanes from dilute gaseous waste streams: mathematical modeling of advanced bioreactor systems, J. Chem. Technol. Biotechnol. 72 (1998) 93–98.
[5] J.W. Barton, K.T. Klasson, L.J. Koran Jr., B.H. Davison, Microbial removal of alkanes from dilute gaseous waste streams: kinetics and mass transfer considerations, Biotechnol. Prog. 13 (1997) 814–821.
[6] M.A. Deshusses, G. Hamer, I.J. Dunn, Behaviors of biofilters for waste air biotreatment. 1. Dynamic model development, Environ. Sci. Technol. 29 (1995) 1048–1058.
[7] M.A. Deshusses, G. Hamer, I.J. Dunn, Behaviors of biofilters for waste air biotreatment. 2. Experimental evaluation of a dynamic model, Environ. Sci. Technol. 29 (1995) 1059–1068.
[8] C. Alonso, M.T. Suidan, B.R. Kim, B.J. Kim, Dynamic mathematical model for the biodegradation of VOCs in a biofilter: biomass accumulation study, Environ. Sci. Technol. 32 (20) (1998) 3118–3123.
[9] C. Alonso, X. Zhu, M.T. Suidan, Parameter estimation in biofilter systems, Environ. Sci. Technol. 34 (11) (2000) 2318–2323.
[10] T.R. Bhat, D. Venkataramanib, V. Ravic, C.V.S. Murty, An improved differential evolution method for efficient parameter estimation in biofilter modeling, Biochem. Eng. J. 28 (2) (2006) 167–176.
[11] G. Spigno, D.M. de Faveri, Modeling of a vapor-phase fungi bioreactor for the abatement of hexane: fluid dynamics and kinetic aspects, Biotechnol. Bioeng. 89 (3) (2005) 319–324.
[12] W.H. Press, S.A. Teukolsky, W.T. Vetterling, B.P. Flannery, Numerical Recipes in C: The Art of Scientific Computing, 2nd ed, Cambridge University Press, 1992.
[13] A.D. Belegundu, T.R. Chandrupatla, Optimization Concepts and Applications in Engineering, Prentice Hall, 1999.
[14] R.L. Haupt, S.E. Haupt, Practical Genetic Algorithms, Wiley-Interscience, 2004.
[15] N.A. Barricelli, Symbiogenetic evolution processes realized by artificial methods, Methodos (1957) 143–182.
[16] J.H. Holland, Adaptation in Natural and Artificial Systems, University of Michigan Press, 1975.
[17] L.J. Park, C.H. Park, C. Park, T. Lee, Application of genetic algorithms to parameter estimation of bioprocesses, Med. Biol. Eng. Comput. 35 (1) (1997) 47–49.
[18] M. Ranganath, S. Renganathan, C. Gokulnath, Identification of bioprocesses using genetic algorithm, Bioprocess Biosyst. Eng. 21 (2) (1999) 123–127.
[19] O. Roeva, A modified genetic algorithm for a parameter identification of fermentation processes, Biotechnol. Biotech. 20 (1) (2006) 202–209.
[20] E.R. Rene, J.H. Kim, H.S. Park, An intelligent neural network model for evaluating performance of immobilized cell biofilter treating hydrogen sulphide vapors, Int. J. Environ. Sci. Technol. 5 (3) (2008) 287–296.
[21] E.R. Rene, S.M. Maliyekkal, L. Philip, T. Swaminathan, Back-propagation neural network for performance prediction in trickling bed air biofilter, Int. J. Environ. Pollut. 28 (4) (2006) 382–401.
[22] S.-H. Lee, Simultaneous Removal of Ethylene and Ammonia using Biofiltration, Purdue University, West Lafayette, 2008.
[23] S.-H. Lee, C. Li, A.J. Heber, C. Zheng, Ethylene removal using biotrickling filters: Part I Experimental description, Chem. Eng. J. 158 (2010) 79–88.
[24] S. Kim, M.A. Deshusses, Development and experimental validation of a conceptual model for biotrickling filtration of H_2S, Environ. Prog. 22 (2) (2006) 119–128.
[25] C.R. Wilke, P. Chang, Correlation of diffusion coefficients in dilute solutions, AIChE. J. 1 (2) (1955) 264–270.
[26] D.S. Reid, in: D.C. Ellwood, et al. (Eds.), Contemporary Microbial Ecology, Plenum, 1981.
[27] R.P. Schwarzenbach, P.M. Gschwend, D.M. Imboden, Environmental Organic Chemistry, John Wiley & Sons, 1993.
[28] Mihran co., Perlite. URL: http://www.perliteco.com/filtration.html, 2006.
[29] U. Sahin, O. Anapali, S. Ercisli, Physico-chemical and physical properties of some substrates used in horticulture, Gartenbauwissenschaft 67 (2) (2002) 55–60.
[30] H.H. Tabak, in: R.E. Hinchee, R.F. Offenbuttel (Eds.), Development and Application of a Multilevel Respirometric Protocol to Determine Biodegradability and Biodegradation Kinetics of Toxic Organic Pollutant Compounds (On-Site Bioreclamation Processes for Xenobiotic and Hydrocarbon Treatment, 1991.
[31] J.S. Devinny, M.A. Deshusses, T.S. Webster, Biofiltration for Air Pollution Control, Lewis Publishers, 1999.
[32] B. De heyder, T.B. Elast, H.V. Langenhove, W. Verstraete, Enhanced ethene removal from waste gas by stimulating nitrification, Biodegradation 8 (1997) 21–30.
[33] L. Elsgaard, Ethylene removal by a biofilter with immobilized bacteria, Appl. Environ. Microb. 64 (11) (1998) 4168–4173.
[34] J. Kim, Assessment of ethylene removal with Pseudomonas strains, J. Hazard Mater. B131 (2006) 131–136.
[35] L.J. Rose, R.B. Simmons, S.A. Crow, D.G. Ahearn, Volatile organic compounds associated with microbial growth in automobile air conditioning systems, Curr. Microbial. 41 (2000) 206–209.